**DAVID ROYLANCE**
Polymers and Composites Division,
Army Materials and Mechanics
Research Center,
Watertown Mass.

# Wave Propagation in a Viscoelastic Fiber Subjected to Transverse Impact

*A dynamical finite-element analysis is used to demonstrate the effect of viscoelastic relaxation on a 3-element rate-dependent model fiber subjected to transverse impact. The transverse shock waves produced by the impact are seen to propagate more slowly and at a larger fiber inclination than the rate-independent theory predicts, and these perturbations are shown to have an appreciable effect on dynamic stress-strain curves which are inferred from measurements of the fiber configuration during impact.*

## Introduction

The problem of transverse impact of a filamentary material has been of continuing interest for approximately the past three decades. This has been due of course to the large number of industrial and military textile applications involving such impacts, but in addition several authors have recently noted that the dynamic constitutive response of a material can be inferred from high-speed photographic measurements of the fiber configuration during the impact. In this latter regard, a series of transverse impact tests over a range of impact velocities can serve as a valuable supplement to such dynamic characterization techniques as Hopkinson bar measurements, and can provide one of the very few presently available methods whereby the stress-strain curve can be obtained for materials in fiber or film form at strain rates corresponding to wave-propagation speeds. The stress-strain curve can be calculated quickly and easily from experimental impact data (a numerical program for a programmable desk calculator is available from the author), but these calculations rely on the rate-independent theory of transverse impact which has been developed by Rakhmatulin [1][1] and others. Since it is desirable to characterize even highly rate-dependent materials, such as polymeric fibers, by this technique, the effect of viscoelastic relaxation on the fiber configuration during impact has been analyzed. This paper presents the results of that analysis. Although this study is specifically intended to extend the applicability of the dynamic characterization technique just mentioned, the numerical technique used is capable of generating certain information not obtainable from the analytical treatments commonly used for uniaxial or transverse propagation, so that the results are of more general interest than this one specific application.

### Rate-Independent Theory

Since the early work of Rakhmatulin and Taylor, several authors have formulated the mechanics of transverse impact, assuming a rate-independent material constitutive response. Reviews of this work can be found in the books of Rakhmatulin [1] and Cristescu [2]. The salient features of this theory can be stated with reference to Fig. 1. Upon impact, longitudinal strain waves are propagated outward from the point of impact. The increments of strain $\epsilon$ comprising these waves propagate at speeds $c(\epsilon)$ corresponding to the slope of the dynamic stress-strain curve at that strain: $c(\epsilon) = \sqrt{dT/d\epsilon} = \sqrt{E(\epsilon)}$. (Here the material density is included implicity by using the textile units of grams/denier for the tension $T$ and the modulus $E$, and numerical conversion factors have been omitted.) Depending on the shape of the stress-strain curve, these strain waves may contain both dispersive and shock components. Behind these waves, material flows inward toward the point of impact at a constant velocity $w$ and strain $\epsilon_0$. In addition to the longitudinal waves, transverse shock waves are propagated outward from the point of impact. This wave usually propagates more slowly than the final longitudinal wavelet, and can usually be characterized as follows: At the transverse wave front, the inward material flow velocity ceases abruptly and is replaced by a transverse particle velocity $v$ equal to that of the projectile. The strain and tension are unchanged across this wave front, but both the longitudinal and

[1] Numbers in brackets designate References at end of paper.

Contributed by the Applied Mechanics Division and presented at the Applied Mechanics Summer Conference, University of California, La Jolla, Calif., June 26–28, 1972, of The American Society of Mechanical Engineers.

Discussion on this paper should be addressed to the Editorial Department, ASME, United Engineering Center, 345 East 47th Street, New York, N. Y. 10017, and will be accepted until April 20, 1973. Discussion received after this date will be returned. Manuscript received by ASME Applied Mechanics Division, August 5, 1971; final revision, November 24, 1971. Paper No. 72-APM-27.

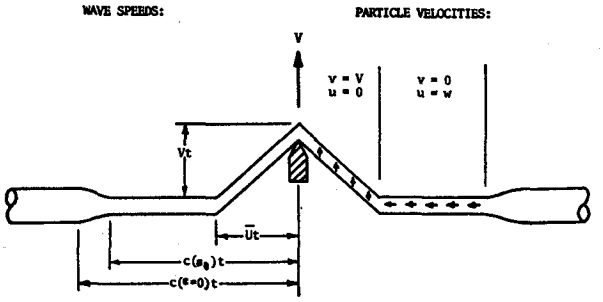


**Fig. 1 Wave propagation in a transversely impacted filament**

transverse particle velocities experience discontinuities there. (The apparently unbalanced tensions on either side of the wave front are compensated by the change in particle momentum as the wave propagates.) Behind the transverse wave front, all particle velocities are equal in magnitude and direction to the projectile velocity, and the yarn configuration is a straight line at a constant inclination $\theta$ from the longitudinal direction.

Smith [3] has presented a comprehensive summary of the rate-independent theoretical relations between these variables, as well as the modifications which are necessary to describe such complications as shock formation and interference between the longitudinal and transverse waves. For a given stress-strain curve and impact velocity $V$, these relations can be used to calculate the final strain $\epsilon_0$, the final tension $T_0$, the longitudinal particle velocity $w$ between the final strain wave and the transverse wave, the transverse wave speed $U$ and $\bar{U}$ (in Lagrangian and laboratory coordinates, respectively), and the fiber inclination $\theta$. Working backward, one can use experimental plots of either $\bar{U}$ or $\theta$ versus $V$ to obtain values of $T_0$, $\epsilon_0$, and $w$ as functions of $V$. The sets of $T_0 - \epsilon_0$ states can then be cross-plotted to produce a dynamic stress-strain curve. Papers by Smith [4] and Schultz [5] illustrate the technique using $\bar{U}$-$V$ and $\theta$-$V$ data, respectively.

The experimental measurements of $\theta$ or $\bar{U}$ are made from photographic exposures taken at times prior to any interactions of reflected longitudinal waves with the transverse wave; these interactions modify both $\theta$ and $\bar{U}$ and render analysis of the data very difficult, if not impossible. While it is experimentally possible to avoid these longitudinal-transverse wave interactions, it may not be possible to obtain photographic records of the fiber configuration sufficiently close to the time of impact such that appreciable viscoelastic relaxation has not occurred. Relaxation causes the plateau of constant strain which the rate-independent theory predicts to exist behind the longitudinal strain waves to be replaced by a field of simultaneously increasing strain (creep) and relaxing stress; in addition the intensity of the strain wave front is attenuated as it propagates along the fiber. These continuing changes in the stress-strain state in which the transverse wave propagates alter the configuration of the impacted fiber from that predicted by the rate-independent theory, and several authors [6–8] have noted discrepancies between the theoretically predicted and experimentally observed impact parameters which seem attributable to relaxation processes. Smith [6] in particular argues that appreciable relaxation occurs during the first 50 microsec after impact of polyester and nylon textile yarns which is essentially complete at longer times; the effects of such relaxation will certainly be present in photographic records, which are taken in the range of approximately 20–200 $\mu$sec after impact.

If dynamic stress-strain curves obtained from $\theta$-$V$ or $\bar{U}$-$V$ data are to have any meaning for rate-dependent materials, the magnitude of the perturbation of the fiber configuration due to relaxation must be assessed. It is not obvious a priori whether application of the rate-independent theory to the relaxing fiber produces grossly erroneous results, or perhaps an approximately valid result. A possible approach to this problem is to use a given time-dependent material response—either a spring-dashpot model representation or experimental dynamic data obtained via time-temperature shifting techniques—and then compare the predicted impact configuration with that of the rate-independent theory. Such a procedure can lead to an estimation of the relative effect of material relaxation and thus assist in determining the error produced when the rate-independent theory is used to characterize a rate-dependent material.

### Prior Work in Viscoelastic Wave Propagation

Several recent papers have addressed the problem of uniaxial wave propagation in a viscoelastic medium, the spring-dashpot representation of material constitutive response being perhaps more common than experimentally measured properties. Lee and Kanter [9] used Laplace transform methods to demonstrate the attenuation of the wave front in a Maxwell solid, and Glauz and Lee [10] later applied the method of characteristics to this same problem. Morrison [11] used Laplace transforms to illustrate wave propagation in a standard linear solid (a spring in parallel with a Maxwell element), and Smith [12] modified this solution for the specific case of longitudinal fiber impact. Knauss [13] obtained a series solution for viscoelastic wave propagation and applied experimental time-temperature reduced relaxation modulus values for Hysol 8705 to it; Wenner [14] had earlier used experimental modulus values in conjunction with a numerical finite-element analysis of uniaxial propagation. Smith [15] has attacked the problem of transverse impact of a viscoelastic fiber using a numerical scheme based on the method of characteristics, and the results of his analysis will be compared with those of the present study.

## Method of Analysis

### Direct Numerical Analysis

In recent years, Davids, et al. [16–18], have developed a dynamical form of finite-element analysis which will be referred to here as "direct analysis." The mechanics of wave propagation are usually formulated by applying an impulse-momentum balance and a condition of continuity to an incremental volume of material; when the size of the volume element is reduced to the limit a system of hyperbolic partial differential equations results which in conjunction with the boundary values and the material constitutive law describes the space-time response of the physical system. The combined system of equations is then attacked by analytical mathematical techniques, such as Laplace transform methods or the method of characteristics, or by replacing the partial derivatives with finite divided differences so as to effect a computational solution using a digital computer. Direct analysis is a computer-oriented technique, but it differs from the finite-difference approach in that the original incremental volume element is never taken to the limit; the fundamental governing relations are used directly and the development of the differential equations is dispensed with.

Direct analysis has several advantages over these other methods: its conceptual simplicity leads to an easily written and debugged computer program, and boundary conditions and constitutive laws can be changed with only very minor program alterations. In addition, phenomena which render analytical approaches hopelessly intractable—such as wave reflections at boundaries, longitudinal-transverse wave interactions, unloading waves, etc.—are incorporated automatically simply by specifying the appropriate boundary conditions.

Criteria for accuracy and stability of the method are related to the theory of characteristics for hyperbolic systems and are similar to those developed for finite-difference methods [19]. Given a wave equation of the form

$$\partial^2 u/\partial t^2 = c^2(\partial^2 u/\partial x^2) \tag{1}$$

which is to be solved numerically by approximating $\partial t$ and $\partial x$ by

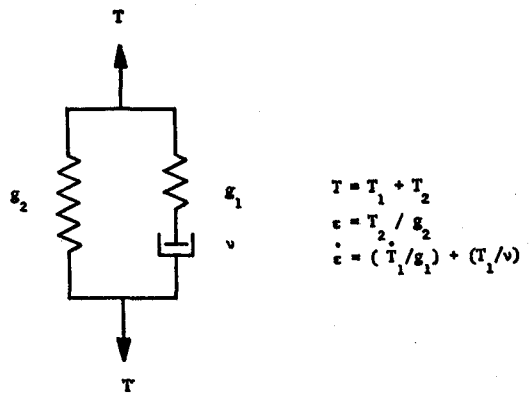


**Fig. 2 Spring-dashpot representation and basic relations for the standard linear solid**

finite differences $\Delta t$ and $\Delta x$, respectively, a "stability ratio" $\alpha$ can be defined as

$$\alpha = c(\Delta t/\Delta x) \tag{2}$$

Courant, et al. [20], have shown that the finite-difference solution is stable and accurate for $\alpha = 1$, stable but increasingly inaccurate for $\alpha < 1$, and violently unstable for $\alpha > 1$. The choices for $\Delta x$ and $\Delta t$ are thus not independent, but are related by the wave speed $c$ for the choice of $\alpha = 1$.

In the direct analysis of the impacted fiber, this criterion is equivalent to adjusting the rate of march of the computer solution along the fiber to match the rate of propagation of the strain wave. Conceptually, this requirement is related to the necessity of programming the finite governing equations so as to model the actual continuous dynamic process as accurately as possible. If a major disturbance—such as the passage of a strain wave with its accompanying energy input—takes place in a finite element which is not considered explicitly in the computational scheme, one can almost be guaranteed increasingly divergent numerical results. This conceptual approach to stability—rather than the formal criteria dictated by the theory of characteristics—is generally more workable in the actual programming of the method. Once a stable computational scheme has been developed, one usually attempts to increase its accuracy to whatever limit is desired by decreasing the size of the finite elements; i.e., by increasing the number of mesh points. Since for $\alpha = 1$, a decrease in $\Delta x$ requires a corresponding decrease in $\Delta t$, the computation time—and therefore the expense—required for analysis of a given impact event increases as the square of the number of mesh points. The mesh size is therefore chosen so as to balance the conflicting requirements of economy and accuracy.

### Choice of Constitutive Law

All numerical results presented here will be for the constitutive response of the standard linear solid, indicated schematically in Fig. 2. Here $\epsilon$ is the strain, $T$ is the tension, the $g$'s are spring constants, and $\nu$ is the dashpot viscosity. Following Smith [12], it is convenient to define the parameters $g$, $\lambda$, and $\tau$ by $\lambda g = g_1$, $(1 - \lambda)g = g_2$, and $\lambda g\tau = \nu$; the constitutive equation can then be written

$$g\dot{\epsilon} + \frac{(1 - \lambda)g}{\tau}\epsilon = \dot{T} + \frac{1}{\tau}T \tag{3}$$

(Here the dots denote time derivatives.) The parameter $g$ represents the instantaneous or glassy modulus of the model, $\tau$ is the relaxation time of the viscous arm, and as $\lambda$ is varied from zero to one the amount of viscous response varies from zero (purely elastic case) to that of a Maxwell element. In a stress relaxation test, for instance, the tension relaxes exponentially from an initial value $T = g\epsilon_0$ to an asymptotic limit of $(1 - \lambda)g\epsilon_0$ in a characteristic time $\tau$.

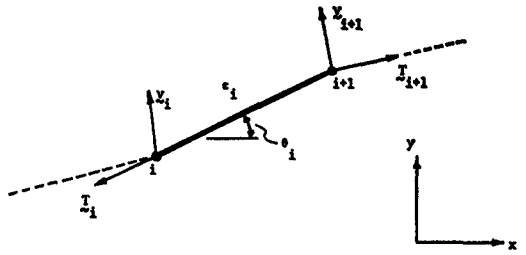


**Fig. 3 Finite-element conceptualization of the fiber**

Equation (3) can be written in finite-difference form as

$$g\frac{\Delta\epsilon}{\Delta t} + \frac{(1 - \lambda)g}{\tau}\epsilon = \frac{\Delta T}{\Delta t} + \frac{1}{\tau}T \tag{4}$$

Letting the subscripts $t$ and $t - 1$ identify the variables $T$ and $\epsilon$ at times after and before the passage of the time increment $\Delta t$, a new value of tension can be computed from the current strain and the previous strain and tension as

$$T_t = \frac{g(\epsilon_t - \epsilon_{t-1}) + [g(1 - \lambda)/\tau]\Delta t\epsilon_t + T_{t-1}}{1 + (\Delta t/\tau)} \tag{5}$$

Equation (5) is in a form readily adapted to the direct analysis program.

The standard linear solid was not chosen for reasons of ease of programming, since either experimental data or much more elaborate spring-dashpot models could have been programmed almost as easily. Such normally intractable elaborations as calculation of adiabatic heating due to the dynamic energy input of the strain wave and the effect of the temperature rise on the constitutive response could also have been easily incorporated. Use of the standard linear solid, however, has several compelling advantages:

1 Being simple and easily visualized, its results help establish an intuitive feeling for the effect of relaxation during fiber impact.

2 Many previous analyses of viscoelastic wave propagation have used the standard linear solid, and its use here permits correlation of the results with these earlier works.

3 Most important, the standard linear solid appears to provide a rather accurate model for the textile yarns being tested in our laboratory. With increasing strain rate, their stress-strain curves become increasingly linear, although there remains the strong evidence mentioned earlier of appreciable relaxation during approximately the first 50 microsec after impact. The specific molecular nature of this relaxation is somewhat unclear, but mechanical loss spectroscopy has indicated that molecular motions on this time scale are available to the material. The standard linear solid provides this linear but time-dependent response.

### Computational Scheme for Transverse Impact

The application of direct analysis to transverse impact has been demonstrated by Lynch [21]; his paper shows that many diverse aspects of the problem can be examined by this method: energy loss of the impacting projectile, energy partition in the impacted fiber, effect of elastic support on the fiber, nonlinear and time-dependent stress-strain curves, and impact of a flexible membrane. His computational scheme was used with only minor modification to analyze the present problem.

A fiber of half-length $L$, to be impacted at zero obliquity at its midpoint with velocity $V$, is considered as consisting of $n$ finite elements as shown in Fig. 3. Associated with the $i$th element are laboratory coordinates $x_i$, $y_i$, a scalar strain $\epsilon_i$, and vector quanti-

ties $\mathbf{T}_i$ tension and $\mathbf{v}_i$ velocity. The tension $\mathbf{T}_i$ has the same direction as the element itself (approximating the fiber's assumed inability to support a bending moment), while $\mathbf{v}_i$ is not restricted in direction. These variables are related by simple governing laws: impulse-momentum balance, continuity, etc. The program is then written so as to employ these relations sequentially and effect a recursive algorithm for proceeding from one element to the next over the length $L$, and then repeating the process at a new increment of time. It was found that satisfactory results were obtained with this very simple idealization of the fiber, and such elaborations as provision for lateral inertia were unnecessary.

Even though the fiber motion takes place in two space dimensions, the computer solution is referenced to a Lagrangian frame attached to and extending with the fiber; this essentially reduces the problem to one dimension. The components of the vector quantities with respect to the laboratory coordinates are computed by means of the element's inclination angle $\theta_i = \tan^{-1} \times [(y_{i+1} - y_i)/(x_{i+1} - x_i)]$. In the summary of the computational scheme, these vector resolutions, as well as all units conversion factors, are omitted for clarity. The material density and the element mass are included implicitly as before by choice of modulus $g$ and tension $T$ in units of force per linear density (grams per denier).

1 Specify input parameters: $n, V, L, g, \lambda, \tau$.

2 Define increment sizes

$$c = \sqrt{g} \tag{6a}$$

$$\Delta L = L/n \tag{6b}$$

$$\Delta t = \Delta L/c \tag{6c}$$

3 Propagation procedure; repeat for $i = 1$ to $i = n$. The value of a variable here is identified with the current or preceding time increment by a second subscript, $t$ or $t - 1$.

(*a*) *Impulse-Momentum Balance*

$$\mathbf{v}_{i+1,t} = \mathbf{v}_{i+1,t-1} + [(\mathbf{T}_{i+1,t-1} - \mathbf{T}_{i,t-1})(\Delta t/\Delta L) \tag{7}$$

(*b*) *Impose Boundary Conditions*

$$\text{If } i = 1, \quad \mathbf{v}_{1,t} = V \tag{8a}$$

$$\text{If } i = n, \quad \mathbf{v}_{n,t} = 0 \tag{8b}$$

(*c*) *Continuity Condition*

$$\epsilon_{i,t} = \epsilon_{i,t-1} + \left\{ \frac{[(\mathbf{x}_{i,t-1} + \mathbf{v}_{i,t}\Delta t) - (\mathbf{x}_{i+1,t-1} + \mathbf{v}_{i+1,t}\Delta t)]}{[\mathbf{x}_{i,t-1} - \mathbf{x}_{i+1,t-1}]} - 1 \right\} \tag{9}$$

(Here $\mathbf{x}_i$ is the coordinate vector corresponding to $x_i, y_i$.)

(*d*) *Constitutive Law (From Equation (5))*

$$T_{i,t} = \frac{g(\epsilon_{i,t} - \epsilon_{i,t-1}) + [(1 - \lambda)g/\tau]\epsilon_{i,t}\Delta t + T_{i,t-1}}{1 + (\Delta t/\tau)} \tag{10}$$

(Here $T$ is the magnitude of the vector $\mathbf{T}$.)

(*e*) *Compute New Laboratory Coordinates of Element*

$$\mathbf{x}_{i,t} = \mathbf{x}_{i,t-1} + \mathbf{v}_{i,t}\Delta t \tag{11}$$

4 Increment time

$$t = t + \Delta t \tag{12}$$

Steps 3 and 4 are repeated for a specified number of times corresponding to the time range of interest, or a failure criterion can be incorporated into the program to terminate computation at a time corresponding to fiber failure.

Neither the formulation of the foregoing governing equations nor their sequential ordering is unique; this scheme represents just one possibility which generates reasonably stable and accurate results. As the number of wave fronts propagating in the fiber increases due to wave interactions, the stability of the method tends to degenerate somewhat. Within the time range corresponding to time-to-break of the impacted fiber; however, the method does provide rather accurate values in comparison to experimental observations. If $\lambda$ is set equal to zero, the method also gives results identical to those of the rate-independent analytical theory for a linear constitutive law. Approximately 2 millisec of computation time are required per element for the CDC 6400 computer system.

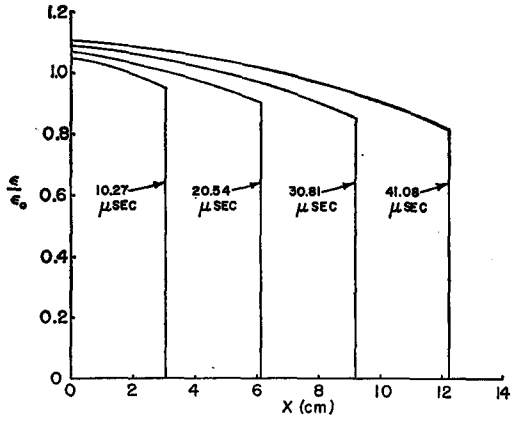


**Fig. 4 Normalized strain plotted against Lagrangian fiber coordinate for various times after impact for material constants $g$ = 100 gpd, $\lambda$ = 0.2, $\tau$ = 50 μsec**

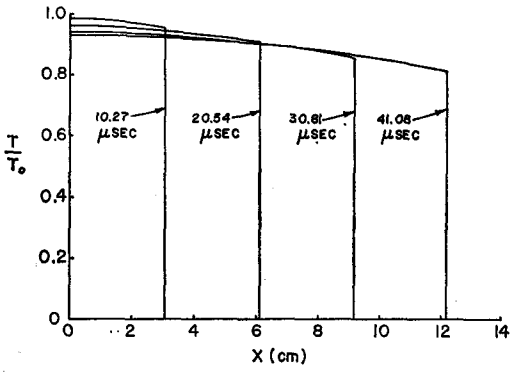


**Fig. 5 Normalized tension distribution along fiber; same units as Fig. 4**

## Results

The direct analysis program generates numerical values for the position, velocity, strain, and tension of each finite element of fiber as a function of time after impact. (The partition of kinetic energy lost by the projectile into fiber kinetic and strain energy is also computed, but these data will not be included here.) Figs. 4 and 5 show the distribution of nondimensionalized strain and tension along the fiber at various times after impact, plotted against the Lagrangian fiber coordinate. These distributions are for a choice of $g$ = 100 *gpd*, $\lambda$ = 0.2, and $\tau$ = 50 μsec; the corresponding longitudinal wave speed is 2970 meters/sec. The values of the ordinates have been normalized by the strain $\epsilon_0$ or tension $T_0$ which the rate-independent analytical theory predicts for a linear material at the same impact velocity $V$. $\epsilon_0$ is found by a numerical solution of the equation

$$V^2 = g\epsilon_0(1 + \epsilon_0) - \left[\sqrt{g\epsilon_0(1 + \epsilon_0)} - \epsilon_0\sqrt{g}\right]^2 \tag{13}$$

Then the initial tension is

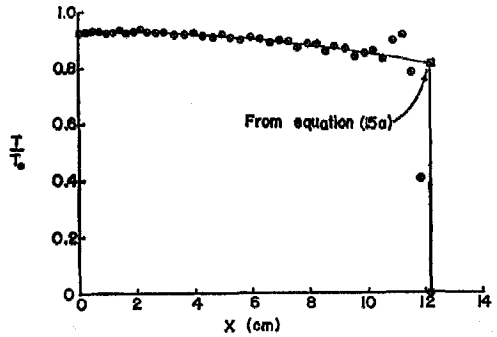


Fig. 6 Numerical values for tension distribution for $t = 41.08$ $\mu$sec after impact; same units as Fig. 4

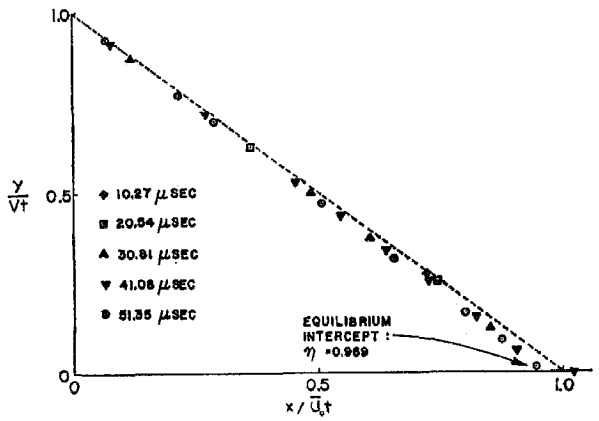


Fig. 7 Normalized transverse wave configuration for various times after impact for material constants $g = 100$ gpd, $\lambda = 0.2$, $\tau = 20$ $\mu$sec

$$T_0 = g\epsilon_0 \tag{14}$$

$T_0$ and $\epsilon_0$ can also be computed by the direct analysis program by setting $\lambda = 0$.

The distributions in Figs. 4 and 5 demonstrate the features noted by several of the previously mentioned authors as being typical of viscoelastic wave propagation: the magnitude of the wave front attenuates as it propagates along the fiber, the strain at a given position increases with time from its original value, and the tension decays with time. Smith [15] used the method of characteristics to show that the wave-front attenuation is given by

$$T(ct, t) = T_0 \exp(-\lambda t/2\tau) \tag{15a}$$

$$\epsilon(ct, t) = \epsilon_0 \exp(-\lambda t/2\tau) \tag{15b}$$

The wave-front tension magnitude predicted by equation (15$a$) is shown in Fig. 6, which also illustrates the numerical accuracy of the direct analysis. (Here a 6-in. fiber was broken into 200 finite elements.) Considerable numerical overshoot is evident at the wave front, but the distribution extrapolates to the analytically predicted value.

By means of Laplace transforms, Smith [12] also obtained approximate expressions for the strain and tension distributions in a longitudinally impacted fiber. These expressions predict that the tension and strain at the point of impact will approach the limiting values

$$T(0, \infty) = T_0\sqrt{(1 - \lambda)} = 0.894T_0 \tag{16a}$$

$$\epsilon(0, \infty) = \epsilon_0/\sqrt{(1 - \lambda)} = 1.118\epsilon_0 \tag{16b}$$

where the numerical values are for $\lambda = 0.2$. At $x = 0$, the distributions in Figs. 5 and 4 approach limiting values greater than

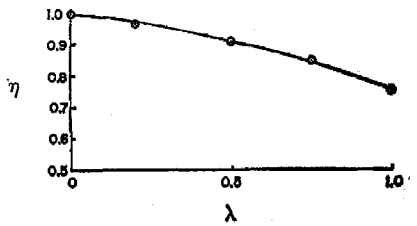


Fig. 8 Variation of relaxation correction factor $\eta$ with model viscous fraction $\lambda$

equation (16$a$) for tension and greater than equation (16$b$) for strain. Thus stress relaxation is slightly less and creep slightly greater for transverse impact than for longitudinal impact; Smith [15] reached this same conclusion in his work on transverse impact.

The effect of relaxation on the experimentally observable quantities $\theta$ and $\bar{U}$ is conveniently illustrated by a nondimensionalized plot of the transverse wave configuration, as shown in Fig. 7. The $y$-coordinate of each fiber element is normalized by the projectile travel distance $Vt$, and the $x$-coordinate by the linear rate-independent analytical prediction for the transverse wave travel distance $\bar{U}_0 t$. The analytical expression for $\bar{U}_0$ is

$$\bar{U}_0 = \sqrt{(1 + \epsilon_0)\epsilon_0 g} - \epsilon_0\sqrt{g} \tag{17}$$

For $\lambda = 0$, the normalized coordinates of all fiber elements plot along the straight line from $(y/Vt) = 1$ to $(x/\bar{U}_0 t) = 1$. Fig. 7 shows that viscoelastic relaxation causes the normalized transverse wave to approach a steady-state configuration below this line in a characteristic time $\tau$. ($\tau = 20$ $\mu$sec in Fig. 7.) No discernible curvature is introduced into the transverse wave by the relaxation, but its propagation speed $\bar{U}$ decreases and its inclination angle $\theta$ increases relative to the initial values $\bar{U}_0$ and $\theta_0$.

At times long in comparison to $\tau$, say $t > 2\tau$, the steady-state transverse wave speed $\bar{U}$ can be written simply in terms of the intercept of the "relaxed" profile in Fig. 7 with the $x/\bar{U}_0 t$-axis. Denoting this intercept by $(x/\bar{U}_0 t) = \eta$,

$$\bar{U} = \eta\bar{U}_0 \tag{18}$$

The relaxed inclination $\theta$ is given by

$$\tan\theta = (V_1/\eta\bar{U}_0) = (\tan\theta_0)/\eta \tag{19}$$

The parameter $\eta$ is thus a quantitative measure of the perturbation of $\theta$ and $\bar{U}$ caused by a given amount of viscoelastic relaxation, and provides a correction factor whereby the initial values $\bar{U}_0$ and $\theta_0$ can be inferred from measurements of the relaxed values.

As $\lambda$ is increased from zero to one, i.e., the viscous relaxation increasing from zero to that of a Maxwell element, the perturbation of $\bar{U}$ and $\theta$ increases and $\eta$ decreases from one to lesser values. $\eta$ was determined as a function of $\lambda$ by a series of plots similar to Fig. 7, each the result of a separate computer run. This functional relationship is displayed in Fig. 8. (At $\lambda = 1$, the Maxwell element, relaxation continues indefinitely; the value shown corresponds to $\eta$ at near $t = 50$ $\mu$sec.)

## Discussion

The previous analysis does not provide a means of assessing the degree and type of relaxation actually taking place in a transverse impact experiment, but rather shows quantitatively how the fiber configuration will be affected by an assumed relaxation model. The choice of a valid model for the dynamic constitutive response of a particular material must be based on some independent evidence; this is a formidable task and thorough discussion of it will not be attempted here. As stated earlier, however, there is considerable justification for considering the standard

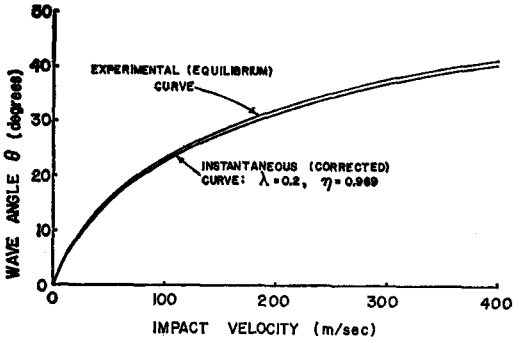


**Fig. 9 Experimental and relaxation-corrected $\theta$-$V$ curves for high-tenacity nylon yarn**

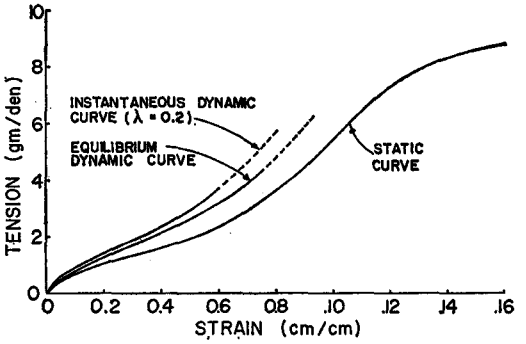


**Fig. 10 Stress-strain curves for high-tenacity nylon yarn**

linear solid as a rather accurate model for the dynamic constitutive response of textile fibers.

Stretching the assumption of the model's validity somewhat farther, it is worthwhile to ask whether the conclusions obtained from the time-dependent but linear model material can be applied to a real material which is both time-dependent and nonlinear. It will be assumed without further argument here that the initial, or instantaneous, values of $\bar{U}_0$ or $\theta$ for a real textile fiber can be inferred to a reasonable approximation from the experimentally measured values by application of the linear-model correction factor $\eta$ just computed. This, in turn, requires that a value of $\lambda$ be assumed, and also assumes that $\tau$ is such that relaxation is essentially complete at the time of the photographic exposure. Given the difficulty of rigorously justifying all these assumptions, the results obtained thereby should be regarded as illustrative rather than exact. Even so, it can be argued that the approximations are reasonable and that the errors are not large.

Fig. 9 shows the experimentally measured variation of $\theta$ with $V$ for high-tenacity nylon yarn, together with the same data corrected for relaxation using equation (19) and $\lambda = 0.2$, $\eta = 0.969$. This latter curve would presumably have been obtained experimentally if the photographs had been exposed at sufficiently short time after impact. The stress-strain curves constructed from these two $\theta$-$V$ curves are shown in Fig. 10, with the static stress-strain curve included for comparison. The dynamic curves are complete to only about half the dynamic breaking strain (estimated to be $\sim$0.15) due to a present lack of higher-velocity experimental impact data, but they clearly show an appreciable difference between the instantaneous and the relaxed data. It should also be mentioned that the corrected $\theta$-$V$ curve in Fig. 9 is not much outside the variation which could occur in the uncorrected curve due to experimental scatter in the individual $\theta$-$V$ measurements.

Since the direct analysis program can incorporate any form of assumed constitutive behavior, the application of relaxation corrections to real materials could be made more realistic as additional information about the actual dynamic material response becomes available. It is likely, however, that such elaborations would be minor corrections, and that the foregoing analysis is sufficient for most purposes. It shows that even though the effects of relaxation are not negligible, the rate-independent procedure for constructing stress-strain curves for transverse impact data is not rendered grossly erroneous by the presence of viscoelastic relaxation, and that the error is of the same order as the experimental scatter.

## References


1 Rakhmatulin, Kh. A., *Strength Under High Transient Loads* (in English), Israel Program for Scientific Translation, Jerusalem, 1966.

2 Cristescu, N., *Dynamic Plasticity*, North-Holland Publishing Company, Amsterdam, 1967.

3 Smith, J. C., McCrackin, F. L., and Schiefer, H. F., "Stress-Strain Relationships in Yarns Subjected to Rapid Impact Loading. Part V: Wave Propagation in Long Textile Yarns Impacted Transversely," *Textile Research Journal*, Vol. 28, 1958, pp. 288–302.

4 Smith, J. C., Fenstermaker, C. A., and Shouse, P. J., "Stress-Strain Relationships in Yarns Subjected to Rapid Impact Loading. Part X: Stress-Strain Curves Obtained by Impacts With Rifle Bullets," *Textile Research Journal*, Vol. 33, 1963, pp. 919–934.

5 Schultz, A. B., "Material Behavior in Wires of 1100 Aluminum Subjected to Transverse Impact," JOURNAL OF APPLIED MECHANICS, Vol. 35, No. 2, TRANS. ASME, Vol. 90, Series E, June 1968, pp. 342–348.

6 Smith, J. C., Fenstermaker, C. A., and Shouse, P. J., "Stress-Strain Relationships in Yarns Subjected to Rapid Impact Loading. Part XI: Strain Distributions Resulting From Rifle Bullet Impact," *Textile Research Journal*, Vol. 35, 1965, pp. 743–757.

7 Petterson, D. R., and Stewart, G. M., "Dynamic Distribution of Strain in Textile Materials Under High-Speed Impact. Part II: Stress-Strain Curves From Strain-Position Distributions," *Textile Research Journal*, Vol. 30, 1960, pp. 422–431.

8 Pilsworth, M. N., and Hoge, H. J., "Rate-Dependent Response of Polymers to Tensile Impact," *Textile Research Journal*, Vol. 35, 1965, pp. 129–139.

9 Lee, E. H., and Kanter, I., "Wave Propagation in Finite Rods of Viscoelastic Materials," *Journal of Applied Physics*, Vol. 24, 1953, pp. 1115–1122.

10 Glauz, R. D., and Lee, E. H., "Transient Wave Analysis in a Linear Time-Dependent Material," *Journal of Applied Physics*, Vol. 25, 1954, pp. 947–953.

11 Morrison, J. A., "Wave Propagation in Rods of Voigt Material and Viscoelastic Materials With Three-Parameter Models," *Quarterly of Applied Mathematics*, Vol. 14, 1956, pp. 153–169.

12 Smith, J. C., "Wave Propagation in a Three-Element Linear Spring and Dashpot Model Filament," *Journal of Applied Physics*, Vol. 37, 1966, pp. 1697–1704.

13 Knauss, W. G., "Uniaxial Wave Propagation in a Viscoelastic Material Using Measured Material Properties," JOURNAL OF APPLIED MECHANICS, Vol. 35, No. 2, TRANS. ASME, Vol. 90, Series E, June 1968, pp. 449–453.

14 Wenner, M. L., "Viscoelastic Waves With Reflection for Longitudinal Impact," *Stress Waves and Penetration*, ed., Davids, N., final report, The Pennsylvania State University, May 15, 1966.

15 Smith, J. C., and Fong, J. T., "On the Coupling of Longitudinal and Transverse Waves in a Linear Three-Element Viscoelastic String Subjected to Transverse Impact," *Journal of Research of the National Bureau of Standards*, Series B, Mathematical Sciences, Vol. 72, 1968, pp. 201–214.

16 Davids, N., Mehta, P. K., and Johnson, O. T., "Spherical Elastoplastic Waves in Materials," *Behavior of Materials Under Dynamic Loading*, ASME, 1965, pp. 125–137.

17 Mehta, P. K., and Davids, N., "A Direct Numerical Analysis Method for Cylindrical and Spherical Elastic Waves," *AIAA Journal*, Vol. 4, 1966, pp. 112–117.

18 Koenig, H. A., and Davids, N., "Dynamic Finite-Element Analysis for Elastic Waves in Beams and Plates," *International Journal of Solids and Structures*, Vol. 4, 1968, pp. 643–660.

19 Crandall, S. H., *Engineering Analysis*, McGraw-Hill, New York, 1956, pp. 396–403.

20 Courant, R., Friedrichs, K., and Lewy, H., "Über die partieller Differenzengleichugen der mathematischen Physik," *Mathematik Annalen*, Vol. 100, 1928, pp. 32–74.

21 Lynch, F. de S., "Dynamic Response of a Constrained Fibrous System Subjected to Transverse Impact. Part II: A Mechanical Model," Technical Report AMMRC TR70-16, Army Materials and Mechanics Research Center, Watertown, Mass., July 1970.